Quantitative Damage Monitoring of Filament Wound Composites by Using Machine Learning-Based Techniques

Bani Mohammad Ali, Amir; Valizadeh Sotubadi, Saleh; Alimirzaei, Sajad; Ahmadi Najafabadi, Mehdi; Pahlavan, Lotfollah

DOI
10.1007/s10443-023-10174-0

Publication date
2023

Document Version
Final published version

Published in
Applied Composite Materials

Citation (APA)
Bani Mohammad Ali, A., Valizadeh Sotubadi, S., Alimirzaei, S., Ahmadi Najafabadi, M., & Pahlavan, L. (2023). Quantitative Damage Monitoring of Filament Wound Composites by Using Machine Learning-Based Techniques. *Applied Composite Materials*, *31 (2024)*(1), 223-247. https://doi.org/10.1007/s10443-023-10174-0

Applied Composite Materials
https://doi.org/10.1007/s10443-023-10174-0

Quantitative Damage Monitoring of Filament Wound Composites by Using Machine Learning-Based Techniques

Amir Bani Mohammad Ali[1] · Saleh Valizadeh Sotubadi[2] · Sajad Alimirzaei[1] · Mehdi Ahmadi Najafabadi[1] · Lotfollah Pahlavan[3]

Received: 29 March 2023 / Accepted: 22 October 2023

Abstract
Composite structures in transportation industries have gained significant attention due to their unique characteristics, including high energy absorption. Non-destructive testing methods coupled with machine learning techniques offer valuable insights into failure mechanisms by analyzing basic parameters. In this study, damage monitoring technologies for composite tubes experiencing progressive damage were investigated. The challenges associated with quantitative failure monitoring were addressed, and the Genetic K-means algorithm, hierarchical clustering, and artificial neural network (ANN) methods were employed along with other three alternative methods. The impact characteristics and damage mechanisms of composite tubes under axial compressive load were assessed using Acoustic Emission (AE) monitoring and machine learning.Various failure modes such as matrix cracking, delamination, debonding, and fiber breakage were induced by layer bending. An increase in fibers/matrix separation and fiber breakage was observed with altered failure modes, while matrix cracking decreased Signal classification was achieved using hierarchical and K-means genetic clustering methods, providing insights into failure mode frequency ranges and corresponding amplitude ranges. The ANN model, trained with labeled data, demonstrated high accuracy in classifying data and identifying specific failure mechanisms. Comparative analysis revealed that the Random Forest model consistently outperformed the ANN and Support Vector Machine (SVM) models, exhibiting superior predictive accuracy and classification using ACC, MCC and F1-Score metrics. Moreover, our evaluation emphasized the Random Forest model's higher true positive rates and lower false positive rates. Overall, this study contributes to the understanding of model selection, performance assessment in machine learning, and failure detection in composite structures.

Keywords Artificial Neural Network · K-means Based Genetic Algorithm · Hierarchical Clustering · Acoustic Emission · Filament Wound Composites · Multilayer Perceptron

✉ Sajad Alimirzaei
alimirzaei69@aut.ac.ir

[1] Department of Mechanical Engineering, Amirkabir University of Technology, Tehran, Iran

[2] Department of Mechanical Engineering – Engineering Mechanics (MEEM), Michigan Technological University, Houghton, USA

[3] Department of Maritime and Transport Technology, TU Delft, Delft, The Netherlands

Published online: 06 November 2023

1 Introduction

Filament winding is one of the most suitable production processes for cylindrical structures, which are usually used to produce tubes, shafts, and pressure vessels, due to controlling the volume fraction of the fibers, and making the desired angles [1]. These structures are subjected to various loads during installation and operation. These loads may be caused by various factors and cause significant internal damage that causes a sharp decrease in the strength at these sections. Therefore, the behavior of composite structures against incoming loads and also the parameters affecting them should be carefully investigated and studied, so that by knowing the behavior of these structures against various types of loading, the reliability of the structure can be increased. In order to investigate the characteristics of energy absorption in composite structures, it is necessary to identify the functional mechanisms of energy absorption and determine the effect of each one on the energy absorption [2]. This issue has led to conducting research on the material properties and identifying damage mechanisms of composite materials due to external loading. The acoustic emission (AE) method is one of the methods used to check the mentioned cases. In the following, the research conducted in the AE field will be reviewed.

Fotouhi et al. [3] investigated the damage mechanisms of glass/epoxy samples with an initial interlayer separation under the three-point bending loading by classifying the AE signals with the C-means method. Ameur et al. [4] investigated and identified failure mechanisms of carbon/flax hybrid composites by AE method. They obtained four classes of AE events by using an amplitude range, the cumulative number of impacts, and energy activity. Beheshtizadeh et al. [5] used wavelet transform and Choi-Williams analysis to determine different failure mechanisms in three-point bending loading. Three types of failure mechanisms, including matrix failure, fiber rupture from the matrix, and fiber breakage were determined and the frequency range of each failure mechanism was determined.

Today, the use of artificial intelligence techniques has been widely considered by many researchers to analyze the data received from experimental tests. In this regard, Jung and Chang [6] proposed a reliable SHM system consisting of an optimal predictive CNN-based model that can perform impact detection by analyzing received signals in smart composite structures. A discrete wavelet transform (DWT) was applied to the impact signals to convert them into input image data for the predictive convolutional neural network-based models. Then, the performance of each optimized neural network model was investigated by comparing the test errors under each applied condition. Azizian and Almeida [7] analyzed the progressive damage of composite structures by developing efficient alternative finite element [8] models built with ANN models and design of experiments (DOE) methods. The response surface method (RSM), combined with FE analysis, was used to generate the dataset. Key results showed that for complex models, ANN metamodels are more accurate than RSM models. Park et al. [9] investigated the design of grid composites with optimization methods based on deep neural networks (DNN). They proposed a multiscale kernel neural network (MNet) that can efficiently predict the strain field within a grid composite subject to external loading. Cui et al. [10] developed a data-driven deep learning (DL) approach based on the convolutional neural network (CNN). The DL technique automatically selects the most sensitive wave features based on the learned training data. In addition, the network's generalization capabilities allow the detection of damage that can be different from the training scenarios. The classification algorithm included batch normalization, mini-batches, L2-norm regularization, and adaptive moment estimation (ADAM) optimization [11] to enhance the performance of both the training phases and

testing phases. The results indicated that the damage-imaging performance depends on the type of signal excitation utilized for the PZT transmitters. Seventekidis and Giagopoulos [12] presented a SHM framework using simulated FE models and a DL CNN hierarchical classifier for a test CFRP pin-joined truss structure.

In other cases, many researchers used machine learning methods to investigate and analyze manufacturing structures [13–15]. Zhao et al. [16] presented the basic theory of modal macro strain-based long gauge distributed sensing technology, and DL theory. Results showed that the proposed deep learning-based approach is a promising way to identify damage types, the location of the excitation load, and support locations, especially when the structural types are complicated and the ambient environment is changing. Due to complexities of composite structures in different shapes and dimensions, the optimal identification and diagnosis of failure mechanisms under various static and dynamic loads by supervised and unsupervised methods is a very challenging issue.

Given the procedural constraints delineated in previous literature, it becomes imperative to employ an appropriate methodology for attaining a more intricate understanding of damage mechanisms. This research endeavors to proactively ascertain the deleterious effects stemming from the progressive failure of composite tubes crafted through the filament winding technique, utilizing AE outcomes as machine learning input via both supervised and unsupervised algorithms. The dataset is scrutinized by implementing an unsupervised Genetic K-means approach, along with hierarchical and supervised ANN models, with the aim of predicting the distinct damage mechanisms arising in each case. A quantitative evaluation of these mechanisms assumes paramount significance in comprehending the energy absorption dynamics within the ultimate structure, thus facilitating the optimization of structures based on efficacious damage mechanisms. Furthermore, to assess the performance of the supervised ANN, the dataset undergoes scrutiny by various alternative algorithms, including Random Forest, SVM, and Naive Bayes. This comprehensive evaluation empowers the identification of the most potent algorithm yielding optimal results in predicting the damage mechanisms. Also comparative analyses encompassing Confusion Matrix, ROC curves, Predicted Class Distribution, ACC, F1-Score, and MCC techniques are employed to assess the individual proficiency of these algorithms in detecting failure mechanisms.

2 Experimental Considerations

2.1 Optimal Energy Absorption

In recent years, achieving an optimal structure in order to absorb maximum energy has been the focus of many researchers, so ferrous, non-ferrous, and composite structures have always been of interest. In the meantime, the major damages in structures are classified into two general groups, catastrophic and progressive damages. In catastrophic failures, we generally see a sharp drop in the force-displacement (FD) diagram after the ultimate tensile strength (UTS) point, and most of the failures in ferrous and non-ferrous metals fall into this category. On the other hand, in composite structures, in the case of precise design with optimal dimensions, the ability of the structure to absorb energy can be increased, so after the UTS, the structure has the ability to carry more load and can withstand failures, in such a way that after the gradual decrease of the force at UTS, an increase in force can be seen again in the FD diagram. This feature has caused the area under the FD diagram in composites to be significantly higher than other metals and makes them a suitable selection for energy absorption.

2.2 Manufacturing Process

In this study, the wet filament winding method, in which a resin bath is used to wet the fibers, has been used to fabricate composite tubes. After checking the wetting angle of resin with fibers, resin viscosity and fiber wetting rate, LR630 resin with LH630 hardener and T-700-24k carbon fiber were selected as the most suitable materials for the manufacturing process. An X-winder desktop winding machine was used to make composite tubes. More details, including the completely described fabrication process of composite samples and composite tubes, are reported in [17].

In order to collect primary data for network training, the AE method, which is a non-destructive method, was used. To monitor the AE activity during the test, an eight-channel AE AMSY-6 and a Vallen System with a maximum sampling frequency of 40 MHz were used. The typical experimental setup of the axial compression testing of the composite tube is shown in Fig. 1. According to this schematic, AE sensors were placed on the composite tube. By compressing the sample under axial loading, the damage is slowly created in the tube, and cracks spread along the longitudinal and transverse directions on the sample's surface. The sensors simultaneously receive the waves caused by the failure and after filtering the waves, transmit them to the computer processing system. Finally, the raw data are analyzed by different methods.

3 Amplitude and Frequency Criteria for Damage Mechanisms

In the operational phase, a composite structure can encounter various forms of damage, encompassing matrix cracking, fiber breakage, fiber/matrix debonding, and delamination [18]. The nature of damage is contingent upon multiple factors, including the direction and rate of loading, the materials constituting the resin and fibers, the arrangement of laminates, the quality of adhesion between the fiber and matrix, as well as environmental conditions such as temperature and humidity. Examination of

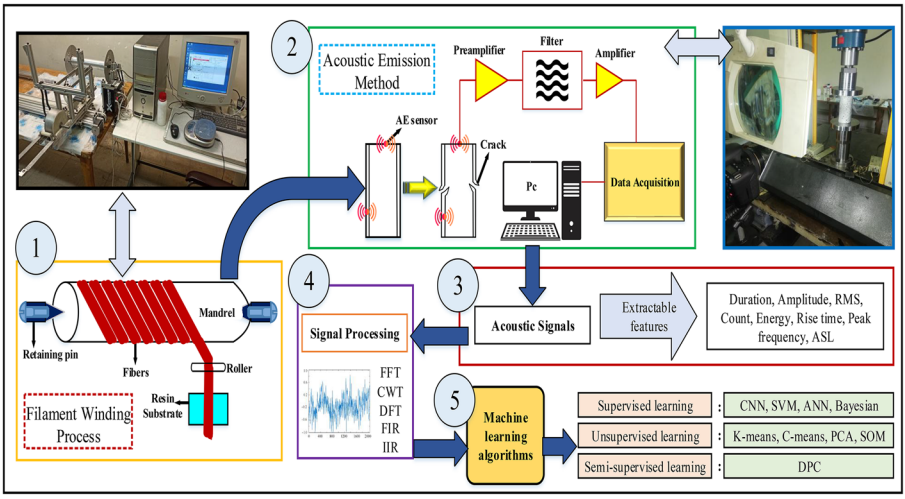

Fig. 1 Sample preparation and research process

existing literature [19] highlights that each damage mechanism observed in composite materials typically yields distinct AE signals. For instance, matrix cracking is commonly characterized by signals exhibiting low amplitude, low frequency, prolonged duration, long rise time, and significant counts.

Conversely, delamination manifests as signals with intermediate amplitude, low frequency, and remarkably long duration. Moreover, fiber breakage is indicated by signals possessing high amplitude, high frequency, and a short rise time [20–23].

Among the multitude of AE features available, such as amplitude, rise time, duration, energy, centroid frequency, and peak frequency, peak frequency, and amplitude are regarded as the most prominent for the purpose of damage identification. Notably, peak frequency demonstrates superior resilience to the attenuation phenomenon, making it a preferable parameter for distinguishing damage compared to amplitude. Table 1. provides an overview of the peak frequency and amplitude reported in existing literature for AE signals associated with various damage mechanisms in diverse composite materials. The observed variations in the reported values for each damage mode can be attributed to factors such as sensor types, loading and boundary conditions, as well as sensor placement. Despite these variations, a consistent finding is that matrix cracking is consistently characterized by the lowest amplitude and frequency, whereas fiber breakage consistently exhibits the highest amplitude and frequency. Delamination and interfacial debonding are typically identified by average values of frequency and amplitude.

In the context of composite tubes, aside from the aforementioned failure mechanisms, SEM images depicted in previous literature demonstrate the occurrence of additional mechanisms such as brooming and kink bands. However, it is crucial to acknowledge that these mechanisms are also induced by the primary failure mechanisms and are not autonomous entities. To gain a deeper comprehension of this matter, Šofer et al. [8] conducted an investigation on the bending loading of composite tubes, providing a comprehensive data that outlines various failure mechanisms as shown in Table 2.

In structures manufactured using the filament winding technique, the occurrence of failure mechanisms associated with inter-layer separation (specifically, fiber/matrix debonding and delamination) is minimized due to the continuous nature of the structure. Moreover, in the event of a catastrophic failure, the occurrence of delamination within the structure is unlikely. However, alternative failure mechanisms may take precedence over the aforementioned mechanisms. Consequently, studying the prevalence of these failure mechanisms allows for the control of the structure's response to various loadings, thereby ensuring optimal performance. By effectively managing interlayer separation failure mechanisms, it is possible to transform the structure's behavior from catastrophic failure to progressive failure. As a result, the structure's capacity to absorb energy and its performance as a shock absorber against axial loads can be significantly enhanced.

4 Data Classification Methods

In this section, numerous strategies that can be used to analyze the AE signals are examined. Since the obtained signals due to the compressive loading of the FW composite tubes are related to various types of failure mechanisms, it's essential to apply methods that can accurately detach the signals. In this study, supervised and unsupervised methods are used for

Table 1 The AE peak frequency (kHz) and amplitude (dB) of various damage mechanisms in Carbon/epoxy materials

Authors	Type of the experiment	Classification of frequency ranges (kHz)				References
		Matrix cracking	Debonding	Delamination	Fiber Breakage	
Nimdum and Renard	Tensile	20–400	30–400	120–360	50–500	[24]
Ni and Iwamoto	Tensile	< 100	200–300	-	400–450	[25]
Saeedifar et al.	Quasi static indentation	< 150	-	150–300	> 400	[26]
Gutkin et al.	Compression	< 50	200–300	50–150	400–500	[27]
Chou et al.	3-point bending	60–120	-	120–210	200–350	[28]
Groot et al.	Tensile	90–180	240–310	-	> 300	[29]
		Classification of amplitude ranges (dB)				
		Matrix cracking	Debonding	Delamination	Fiber Breakage	
Nimdum and Renard	Tensile	60–100	45–65	60–95	< 60	[24]
Liu et al.	Open hole tensile	40–60	50–70	60–80	80–100	[30]
Ceysson et al.	3-point bending	About 48	-	About 63	-	[31]
Bourchak et al.	Fatigue	60–78	-	76–90	-	[32]

Table 2 AE signal characteristics for damage mechanisms in carbon fiber-reinforced polymer (CFRP) composite tubes

Damage Mechanism	AE Signal Characteristics		
	Amplitude (dB)	Duration (μs)	Frequency (kHz)
Fiber break	50–100	100–10,000	300–700
Matrix micro cracks	30–40	< 1000	100–250
Matrix micro cracks (propagation)	40–80	1000–10,000	100–250
Delamination	> 70	1000–10,000	250–300
Debonding	< 60	-	About 300

detecting signals caused by various failures. In fact, these methods of classifying AE signals are related to machine learning methods.

In the supervised learning method, the system is given a set of input–output pairs and the system tries to learn a function that transforms the input into the output. Supervised learning needs some input data in order to train the system.

In this study, supervised and unsupervised methods are used to classify and separation of received signals. The Genetic K-means and hierarchical methods, are used for classification in an unsupervised method, and ANN method is used for classification in a supervised method. By choosing the best classification method, a more accurate diagnosis of each of the failure mechanisms is possible. In the following, the results obtained from each of the data classification methods will be discussed.

4.1 Genetic K-means Cluster

Genetic K-means is a classification method that tries to classify the data in such a way that the ratio of the total distance of the data within a group to the distance between the centers of the groups is minimized [33]. The k-means algorithm has two steps. This algorithm first randomly selects the center of the primary clusters according to Eq. (1), and each data point is assigned to a cluster with the nearest cluster center. In the second step, according to Eq. (2), the new center of each cluster is updated to the mean amount of all the data points that are inside the cluster, where $C_i^{(t)}$ is cluster i and $m_i^{(t)}$ is the center of cluster i at iteration t [34].

$$C_i^{(t)} = \{X_n : \left\|X_n - m_i^{(t)}\right\|^2 \leq \left\|X_n - m_j^{(t)}\right\|^2 \forall j, 1 \leq j \leq k\} \tag{1}$$

$$m_i^{(t+1)} = \frac{1}{\left|C_i^{(t)}\right|} \sum_{X_j \in C_i^{(t)}} X_j \tag{2}$$

4.2 Hierarchical Cluster

The hierarchical pattern is executed in one of two figures: divisive and agglomerative. In the divisive method, each data point is initially considered a cluster. Then, the algorithm detects the two nearest clusters and develops a new cluster containing both data points. The algorithm calculates the distance between the new cluster and the old one again and

combines the two closest clusters. This process is continued to reach the eligible number of clusters. The agglomerative procedure is exactly the reverse of the divisive. The disadvantage of the hierarchical pattern is the low rate of the clustering process [35, 36].

5 Machine Learning Methods

5.1 ANN Method

In addition to the previous attempt to classify the failure type of the composite tubes, supervised learning methods were used as a secondary approach for the classification task of determining the composite failure under the compression forces. For this purpose, ANNs were used to train the machine learning model for the classification tasks. Figure 2, illustrates a schematic of a typical ANN. As the figure illustrates, an ANN is basically comprised of several layers, each consisting of several computation units. The computation units of any ANN with Multi-Layer Perceptron (MLP) architecture are constituent of several linear algebraic units (Eq. (3)) followed by nonlinear computations (Eq. (4)).

$$x_n^j = \sum_{i=1}^{m} w^i x^i + b_n^j \tag{3}$$

$$ReLU : f(x) = \begin{cases} 0. \; x < 0 \\ x. \; x \geq 0 \end{cases} \tag{4}$$

In Eq. (3) x_n^j represents the n^{th} neuron in the j^{th} hidden layer, while x^i represents each of the neurons in the preceding layer. Additionally, w^i represents the weights connecting the neurons of the i^{th} layer with the neurons of the j^{th} layer in the neural network, while b_n^j is the bios term for the n^{th} neuron in the j^{th} layer. Equation (4) illustrates the nonlinear computation unit followed by the linear algebraic computation.

As mentioned above, ANNs were used as an attempt to classify the failure types of the composite tubes. For this purpose, an ANN with the MLP architecture was modeled and developed using the Tensor flow-Keras library in Python programming language. Table 3.

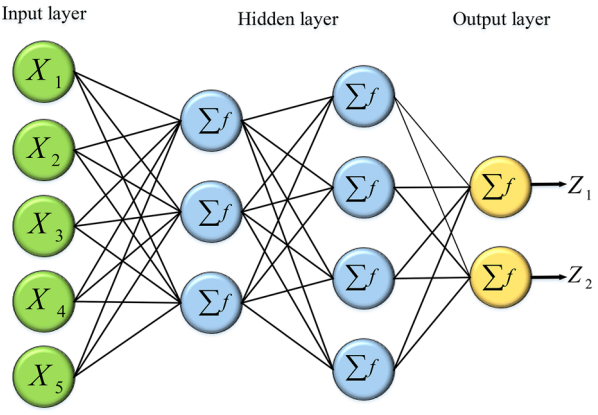

Fig. 2 A scheme of an ANN with MLP architecture

provides information about the network architecture developed in this study. Furthermore, the scheme of the network architecture is represented in Fig. 3.

5.2 Random Forest Classifier Method

The Random Forest Classifier is an ensemble learning technique that uses a collection of decision trees for classification tasks. It is applicable to both binary and multi-class classification and is known for its computational efficiency, resilience to noisy data, and ability to capture nonlinear relationships. Each decision tree in the ensemble individually predicts the class label for a new input, and the Random Forest combines the votes from all trees to assign the predicted class label.

5.3 Naive Bayes Method

Naive Bayes is a classification algorithm based on Bayes' theorem. It calculates the conditional probability of a class given the observed features. Naive Bayes assumes feature independence, making it suitable for tasks like text classification, document categorization, spam filtering, and sentiment analysis. It estimates prior probabilities and likelihoods from training data and uses Bayes' theorem to calculate posterior probabilities for classification. It is simple, efficient, and effective for high-dimensional datasets.

5.4 SVM Method

SVM is a powerful supervised learning algorithm used for classification and regression. It is particularly effective in cases with complex or non-linear decision boundaries. SVM finds an optimal hyperplane that separates data points of different classes with the largest possible margin. It formulates an optimization problem using a hinge loss function and a regularization term. The kernel trick allows SVM to handle non-linear decision boundaries efficiently. The decision function is determined by support vectors, which are the data points closest to the hyperplane.

Table 3 The architecture of the Neural Network developed for failure mechanism classification

	Number of Neurons	Activation Function	Dropout Layer Percentage	Batch Normalizor
Input Layer	2	-	-	Not Utilized
First Layer	20	ReLU	30%	Utilized
Second Layer	15	ReLU	25%	Utilized
Output Layer	4	Softmax	-	Not Utilized

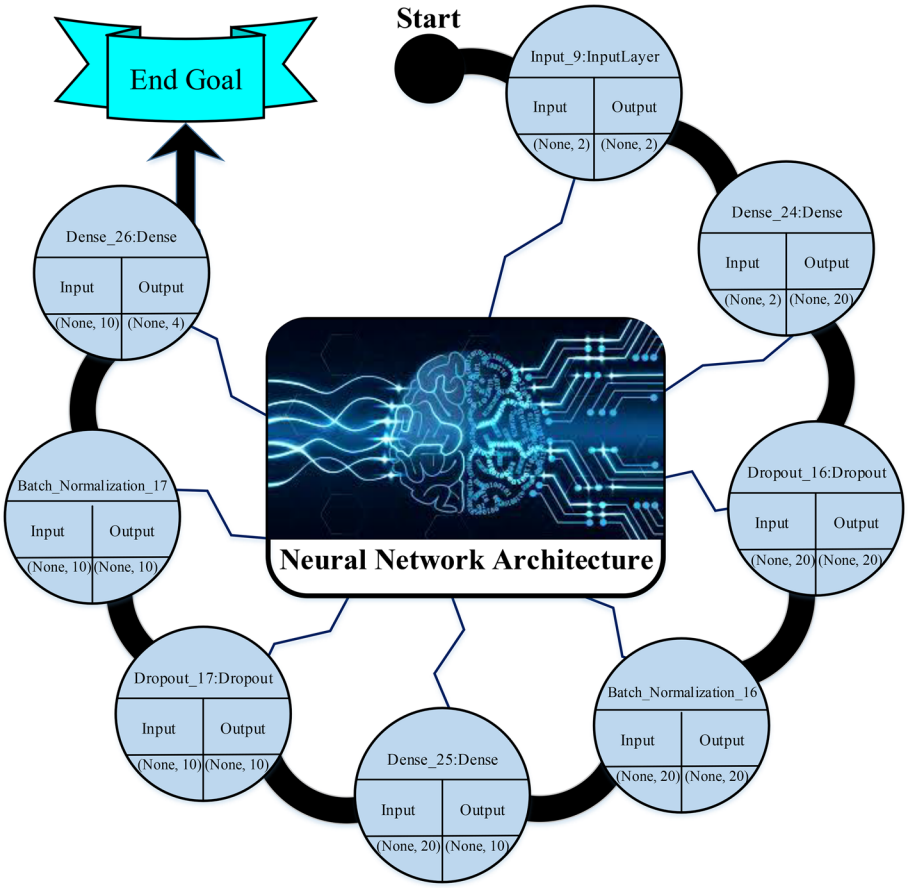

Fig. 3 Neural network architecture used in supervised method

6 Results and Discussion

In this section, the obtained results of unsupervised and supervised methods are investigated. Thereupon quasi-static compressive loading of the composite tubes and receiving the AE signals, the data is filtered to separate the best-received signals. In the following, the results of these methods will be examined.

6.1 Results of Unsupervised Methods

According to the sophisticated terms between various features of AE signals, the process of acoustic data clustering is commonly done by machine learning-based methods. One of the methods of classification of failure mechanisms is the use of unsupervised methods. By reviewing the literature, it is obvious that the privileged parameters for classifying AE date are amplitude and frequency. Hereupon, in order to categorize the AE signals,

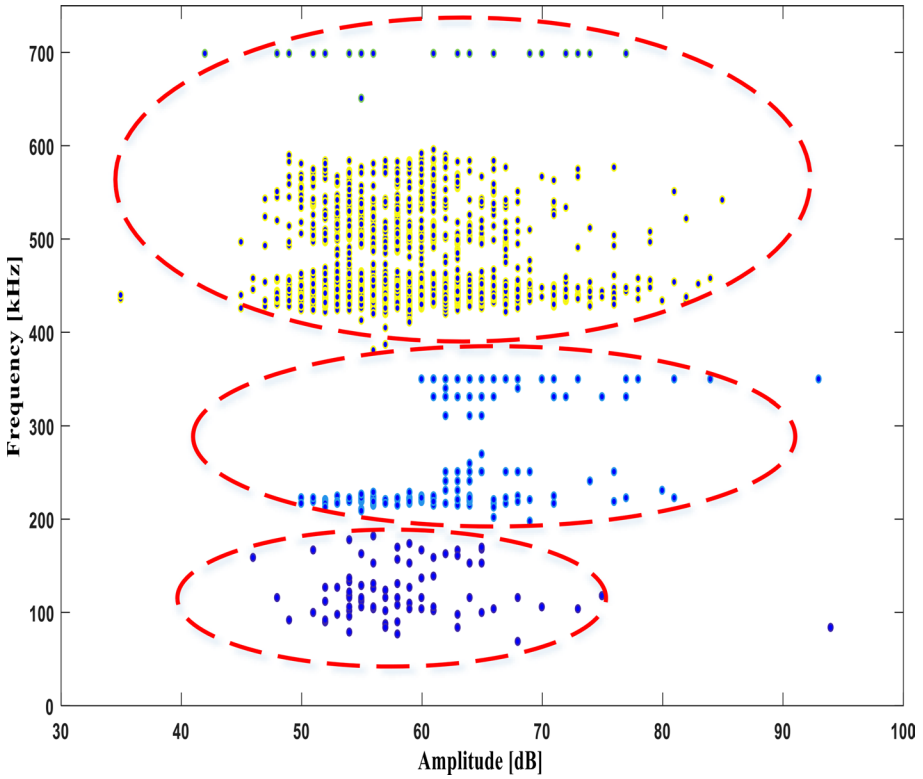

Fig. 4 Hierarchical method

these two parameters were opted from among other AE specifications. As can be seen from Fig. 4, in the hierarchical classification method, the signals relevant to the first cluster were identified with a range of 46–81 dB, with a frequency range of 68 to 200 kHz. Also, the second cluster was specified with an amplitude range of 50–81 and 61–93 dB and a frequency range of 210–350 kHz. Finally, the third cluster was demonstrated by signals with an amplitude range of 45–85 dB and frequencies with a range of more than 380 kHz. The next step is to apply these categories to the interlaminar and intralaminar failure mechanisms. Although there are remarkable differences among the frequency ranges stated for the failure mechanisms in the literature, which is mainly due to the usage of AE systems with different characteristics, however, the common trait of most of the executed research is that the lowest range of the frequency is related to the matrix cracking and the highest frequency range is related to fiber breakage, and the frequency range of interlaminar separation is between these two limits [27, 29, 37]. Therefore, the categories of AE signals are assigned to the failure mechanisms as follows:

First class, which has the lowest frequency, refers to matrix cracking. Third class, with the highest frequency, is assigned to fiber breakage, and the second class, which has a frequency between these two categories, is assigned to interlaminar separation. By comparing the second group of received signals, it can be seen that in the progressive failure mode, two different types of received signals were obtained in the range of 50–81 dB and 61–93 dB. It seems that these two received signal ranges belong to various failure mechanisms. Also,

it seems rather challenging to distinguish between the failure mechanisms of fiber-matrix debonding and delamination, as both failure mechanisms are the same frequency spectra.

The examination of the morphology of composite tubes under compressive load demonstrated that in the progressive failure mode due to the layered bending, the failure initiates from the top of the sample and continues in the form of petals with delamination. Therefore, in the progressive failure mode, both failures including fiber separation from the matrix and delamination occurs simultaneously. The literature demonstrates that the amplitude range of received signals from the failure phenomenon of delamination is greater than the fiber/matrix debonding [8, 19]. Therefore, to further investigate the possibility of distinguishing between these areas, the Genetic K-means algorithm was used to classify the data, and finally, the middle interval was divided into two categories with different amplitude domains.

As can be seen from Fig. 5, the Genetic K-means algorithm divides the frequency range of the progressive failure mode into four clusters with ranges of 68–166 kHz, 173–269 kHz, 310–386, and a cluster with frequencies greater than 404 kHz. It seems that the amplitude range of 50–81 dB is related to the separation of fibers from the matrix and the amplitude range of 61–93 dB is related to interlaminar separation. As can be seen from the above figures, it seems that the prediction of both methods, the hierarchical and Genetic K-means methods, are close to each other for the catastrophic failure mode and there is a good agreement between the results. However, in the progressive failure mode, it was observed that the

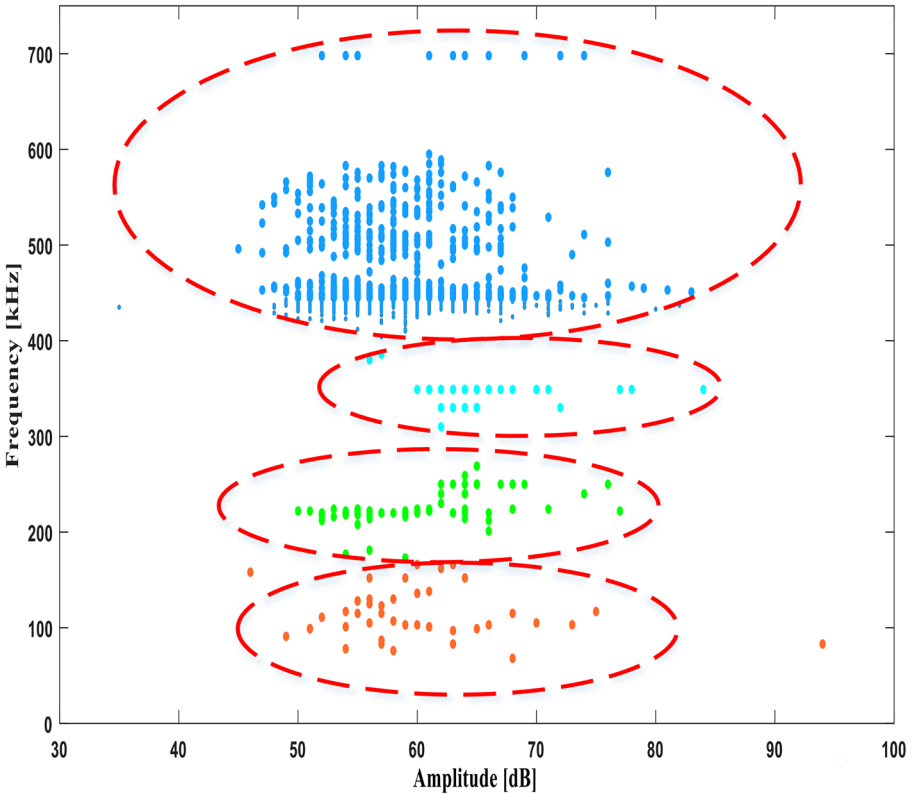

Fig. 5 Genetic K-means method

Genetic K-means algorithm showed a much more accurate prediction than the hierarchical method, so with this method, the failure modes of delamination and fiber/matrix debonding can be separated to each other.

6.2 Results of Supervised Methods

Before the training process, the data was undergone a preprocessing procedure. For this purpose, the input features (frequency and amplitude) were normalized and the data was labeled into four distinct classes each representing a different mechanical failure behaviors. Then the data was split into three subsets known as the training set, the validation set, and the test data set. The training and the validation datasets were fed to the network during the training process, whereas the test dataset was kept out of reach until the training process of the network was done. Then the network was exposed to the test dataset to evaluate the performance of the network and determine how accurate the network could classify the failure mechanisms given the frequency and the amplitude values as input features of the network. The network was comprised of a total of 4 layers. The activation functions usedfor the hidden layers was the ReLU function as described by Eq. (4). However, the function used at the output layer was the Softmax function which took care of the multiclass classification tasks. (Eq. (5))

$$S(x_i) = \frac{\exp(x_i)}{\sum_{j=1:n}\exp\,(x_j)} \tag{5}$$

where, $S(x_i)$ in Eq. (5) represents the probability of the occurrence of each class predicted by the neural network. $\exp(x_i)$ is the probability of the occurrence of the i^{th} class in the network and the term in the denominator ($\sum_{j=1:n}\exp(x_j)$), is the sum of the likelihood of all the classes in the network. Since the problem at hand was a multiclass classification problem, categorical cross entropy function (Eq. (6)) was utilized as the loss function to calculate the cost of the predictions made by the network after every turn (epoch) during the training process.

$$L = \frac{1}{N}\sum y_i \log(\hat{y}_i) + (1 - y_i)\log(1 - \hat{y}_i) \tag{6}$$

In Eq. (4), y_i is the actual class of the i^{th} instance in the training data, while $\hat{y}_i$ is the estimated class predicted by the neural network after each training epoch. Furthermore, N refers to the total number of training and validation datasets. For the training process to be accurate, Adam optimizer, as illustrated in Eqs. (7) – (10), was used as optimization method during the backpropagation for the learning process to be complete after each epoch was done. Table 4. provides information about the hyperparameters used in this study for the training process of the ANN.

Table 4 Selected hyperparameters during the training process of the ANN

α	β_1	β_2	N	η
Learning Rate	Adam optimizer parameter	Adam optimizer parameter	Number of Epochs	Batch size
0.001	0.99	0.95	100	8

$$v_t = \beta_1 \cdot v_{t-1} - \left(1 - \beta_1\right) \cdot g_t \tag{7}$$

$$s_t = \beta_2 \cdot s_{t-1} - \left(1 - \beta_2\right) \cdot g_t^2 \tag{8}$$

$$\Delta w_t = -\alpha \frac{v_t}{\sqrt{s_t + \epsilon}} \cdot g_t w_{t+1} \tag{9}$$

$$\Delta w_t = -\alpha \frac{v_t}{\sqrt{s_t + \epsilon}} \cdot g_t w_{t+1} = w_t + \Delta w_t \tag{10}$$

In Eqs. (7), and (8), β_1, and β_2 are the hyperparameters of the Adam optimizer. v_t, and s_t are the exponential average of gradients along w^j, and exponential average of square of gradients along w^j. g_t describes the gradients of the weights of each layer at time t. In Eq. (9), α is the learning rate defining the rate at which the weights of the neural network are updated at each epoch. Also, ϵ in Eq. (9), is the hyperparameter decreasing the effects of the initial learning rate (α) as the training process of the neural network progresses. Finally, Eq. (10), updates the weights of each layer in the ANN during the backpropagation process during each training epoch.

The network was trained on a system with 11,320 H 3.2 Gb Core i5 CPU, and DDR4 16 Gb RAM for 100 epochs with other specifications provided in Table 4. During the training process, both the training and the validation datasets were fed to the network for the purpose of training. After the training was done, the network achieved a 0.266 loss value on training dataset and a loss value of 0.0406 on the validation datasets. To better evaluate the performance of the network during the training, accuracy metrics was used resulting in a training accuracy of 91.18% while the final validation accuracy was 98.69%. The details of the training process is illustrated in Fig. 6. In Fig. 6, the plot on the left depicts the loss function evolution for both the training and the validation datasets, meanwhile, the plot on the right represents the evolution of the accuracy metrics for the training and the validation datasets.

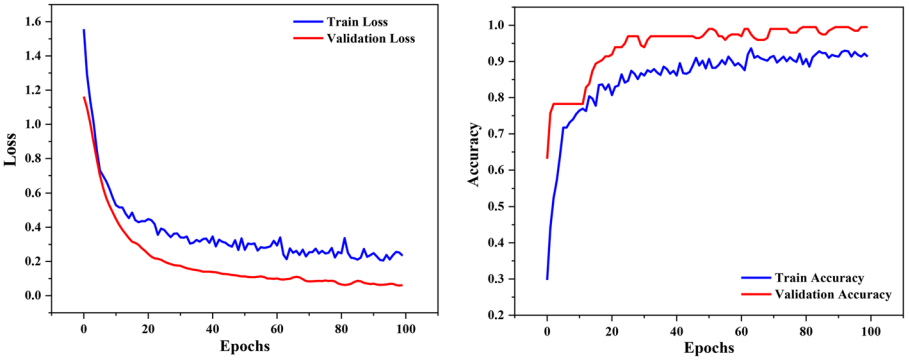

Fig. 6 Loss function and Accuracy evolution of the training and validation data during the training process of the neural network

Algorithm. 1 Pseudocode describing the learning hierarchy in ANN

Initialize learning rate ($\alpha \leftarrow 0.001$)
Initialize Adam Optimizer parameters ($\beta_1 \leftarrow 0.99$, $\beta_2 \leftarrow 0.95$)
Define Training epochs ($N \leftarrow 100$) and learning batch size ($\eta \leftarrow 8$)
Preprocess learning data
Divide learning data into training, validation, and test datasets
Initialize i: $i \leftarrow 1$
While $i < N$
Feed batches of training data into the ANN for forward propagation based on Eqs. (3), and (4)
Make predictions based on the provided input features based on Eq. (5)
Calculate loss based on Eq. (6)
Calculate gradients of each layer using the chain rule
Update weights during the backpropagation based on Eqs. (7) – (10)
Feed the validation data to evaluate the network performance after each training epoch
Calculate validation loss based on Eq. (6)
$i \leftarrow i + 1$
End While
Feed test data to the fully trained network to evaluate the network performance on the test data

After the training procedure of the ANN was completed, the network performance was evaluated by feeding the test dataset to the trained model. Similar to the training and validation datasets accuracy metrics was used to illustrate the performance of the network. To enhance the assessment and estimation of the performance of the ANN model, additional machine learning models, including SVM, Naive Bayes, and Random Forest, were employed. This approach aimed to provide comprehensive insights into the applicability and effectiveness of these models alongside the ANN. Figure 7, shows the confusion matrix of the trained machine learning models on the test dataset.

As represented on the Fig. 7, the horizontal axes shows the number of actual instances while the vertical axes is the instances predicted by the network. The numbers on the main diameter of the matrix refer to the instances where the network successfully predicted the correct class for each input. However, all the other numbers appearing anywhere except the main diameter are the instances where the network failed to predict the class of the corresponding input features correctly. Upon careful examination of the various components depicted in Fig. 7, it becomes evident that the Random Forest model outperforms the other learning models, exhibiting only one misclassification at the boundary between fiber breakage and delamination. Notably, the Random Forest model demonstrates the lowest error rate in the sub-diameter categories, surpassing both ANN and SVM models. Conversely, the ANN and SVM models exhibit the highest error rates, with four misclassifications in diagnosing boundaries between matrix cracking and debonding, and one misclassification in the boundary of fiber breakage with delamination, thus indicating their subpar performance. Furthermore, the Naive Bayes model achieves the second lowest error count, signifying its relatively favorable performance. Consequently, following the Random Forest model, Naive Bayes demonstrates a commendable ability to accurately identify data.

Using the information provided in the confusion matrix, the accuracy of the network on the test dataset was calculated based on Eq. (11):

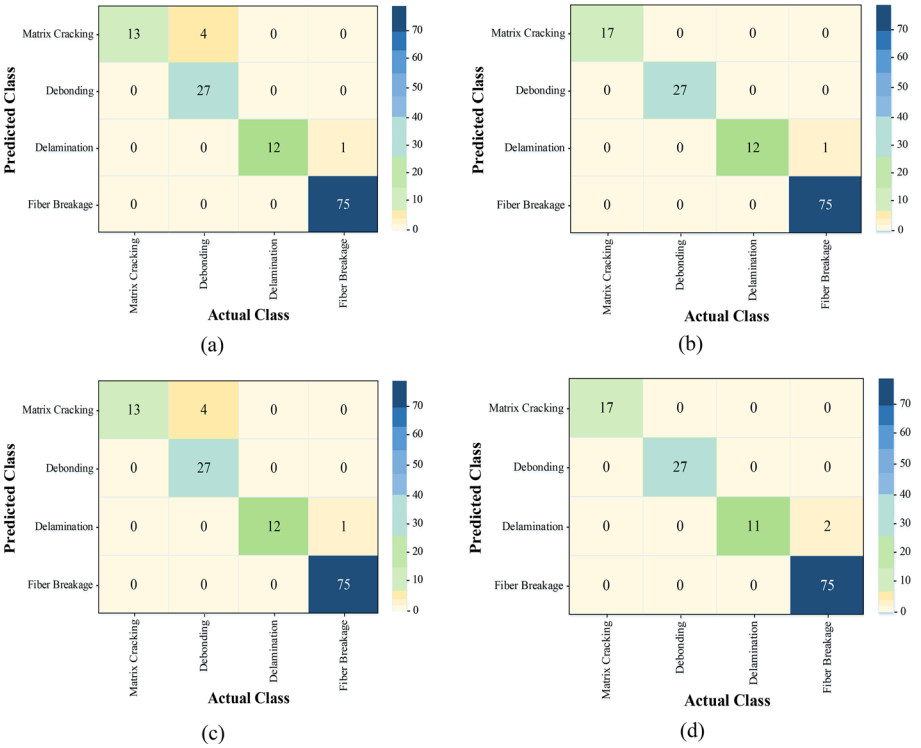

Fig. 7 Confusion matrix representing the performance of the trained **a** ANN, **b** Random Forest, **c** SVM, and **d** Naive Bayes on the test dataset

$$ACC = \frac{TP + TN}{TP + TN + FP + FN} \tag{11}$$

Given the binary nature of the classification task, the model's predictions were categorized into four distinct groups: True Positive (TP), True Negative (TN), False Positive (FP), and False Negative (FN). The TP and TN categories denote the accurate identification of data points belonging to the positive and negative classes, respectively, as confirmed by the machine. Conversely, FP signifies instances where the machine incorrectly classified negatives as positives, while FN represents cases where the machine misclassified positives as negatives. The ACC amount of the models are provided in Table 1, alongside another metric factor.

ACC represents the model's ability to correctly classify instances. Although ACC offers a direct quantitative measure of model performance, an alternative metric, known as the Matthews Correlation Coefficient (MCC), has also been introduced for assessing model performance. MCC, which ranges from -1 to 1, was employed in evaluating the models. Equation (12) defines the MCC criterion. As the MCC criterion approaches the upper limit of its range, it is anticipated that the model's performance will improve.

$$MCC = \frac{TP.TN - FP.FN}{\sqrt{(TP + FN)(TP + FP)(TN + FN)(TN + FP)}} \tag{12}$$

As shown in Table 5, among the models tested, the Random Forest model exhibits the highest performance, achieving remarkable ACC and Mean MCC values of 99.24% and 0.993, respectively. These results indicate the superior predictive capabilities of the Random Forest model compared to other models. Furthermore, the MCC values obtained for the remaining models also exhibit reasonable performance, suggesting their effectiveness in the given context. However, it is noteworthy that ANN and SVM models display lower MCC values compared to the other models. This observation highlights the superiority of the alternative models over the ANN and SVM models in terms of predictive accuracy and reliability.

The overall quality of damage classification is assessed by accuracy. Given the presence of sample imbalance, Precision was employed to appraise the quality of positively predicted true positives, while Recall was employed to evaluate the quality of positive predictions. The computation of the F1 score, a harmonic mean between precision and recall, yielded a value ranging from 0 to 1. The calculations proceeded as outlined below:

$$Precision = \frac{TP}{TP + FP} \tag{13}$$

$$Recall = \frac{TP}{TP + FN} \tag{14}$$

$$F1 - score = \frac{2 \times (Precision \times Recall)}{Precision + Recall} \tag{15}$$

Table 6 presents the calculated mean F1-scores for Random Forest, Naive Bayes, Support SVM, and ANN models. Notably, Random Forest exhibited a mean F1-score of 0.9705, surpassing the other models. Naive Bayes achieved a commendable mean F1-score of 0.9581, followed by SVM with a value of 0.9102, and ANN with 0.9073. These high mean F1-score values, all exceeding 90%, attest to the exceptional classification potential of the models across various types of acoustic emission raw sequence data associated with matrix cracking, debonding, delamination, and fiber breakage in composite materials. Upon meticulous examination of the data, a conspicuous similarity emerges between the trend displayed by the F1-Score criterion and the MCC criterion across the models. Hence, it is evident that both these criteria can be employed as reliable and complementary methods for the evaluation of the models.

Table 5 Various quantitative metrics using the performance of the trained models on the test data

Models	MCC				Mean MCC	ACC
	Matrix Cracking	Debonding	Delamination	Fiber Breakage		
ANN	0.8859	1.0	0.9614	1.0	0.9618	96.21%
Random Forest	1.0	1.0	0.9720	1.0	0.9930	99.24%
SVM	0.8497	1.0	0.9614	1.0	0.9528	96.08%
Naive Bayes	1.0	1.0	0.9410	1.0	0.9850	98.48%

Table 6 F1 - Score metric using the performance of the trained models on the test data

Models	F1 - Score				Mean F1 - Score
	Matrix Cracking	Debonding	Delamination	Fiber Breakage	
ANN	0.7869	1.0	0.8541	1.0	0.9102
Random Forest	1.0	1.0	0.8821	1.0	0.9705
SVM	0.7752	1.0	0.8541	1.0	0.9073
Naive Bayes	1.0	1.0	0.8324	1.0	0.9581

In addition to the accuracy metrics, the Receiver Operating Characteristic [38] curve for each of the classes was extracted using the multiclass ROC technique. ROC curve is a graph representing the performance of the network on each of the classes. The ROC curve is extracted based on two parameters known as the True Positive Rate (TPR), and False Positive Rate (FPR). These parameters represent the instances where the network makes a correct and incorrect predictions for each input instance, respectively. Figure 8, shows the ROC curve for each of the classes each representing a certain failure mechanisms. The dashed line in the middle shows the performance of the untrained network on each failure class, while the curve shows the actual performance of the network on each of the classes after the network is trained.

Along with the ROC curve, the Area Under Curve (AUC) was calculated for each of the classes. An AUC is a metric to evaluate the performance of the network on each classes and can be extracted from the ROC curve. The AUC can take any number within the range of 0 and 1 with 0 being the least accurate performance and 1 being the highest performance accuracy. The AUC values were calculated for each of the classes separately and reported on the ROC curve of each of the classes.

As depicted in Fig. 8, the ROC curves of the Random Forest model closely resemble the ideal state. Notably, in three out of the four scenarios, the area under the curve reaches 1, indicating the model's remarkable performance in accurately detecting each failure criterion. The Naive Bayes model's curve also exhibits a similar performance to that of the Random Forest model. However, it is slightly less effective in detecting delamination damage, as evident from the divergence in the green curve. Conversely, the ROC curves of the ANN and SVM models showcase smaller areas under the graphs, particularly in the blue curve corresponding to Matrix Cracking. This observation highlighted the limitations of these models in effectively distinguishing data associated with this failure mechanism, which aligns well with the findings of the Confusion Matrix analysis.

Additionally, the performance of the networks on the test dataset is visualized in Fig. 9. The plots on the right represent the real distribution of the data in the input feature field. Whereas, the plots on the left show the predicted classes. As shown in the Fig. 9, the networks were capable of correctly classifying the instances where the input features were distinctively different from each other. On the other hand, the networks were prone to incorrectly classify the instances where the input features of the data were similar to the input features of the opposing class. Upon scrutinizing the actual and predicted patterns, it became evident that the presence of color disparities among data points within each model corroborated the findings derived from the Confusion Matrix and ROC curves. For instance, in the Random Forest model, the Confusion Matrix illustrated a solitary detected error in the sub-diagonal of the matrix, as showcased in Fig. 9b, thereby signifying its

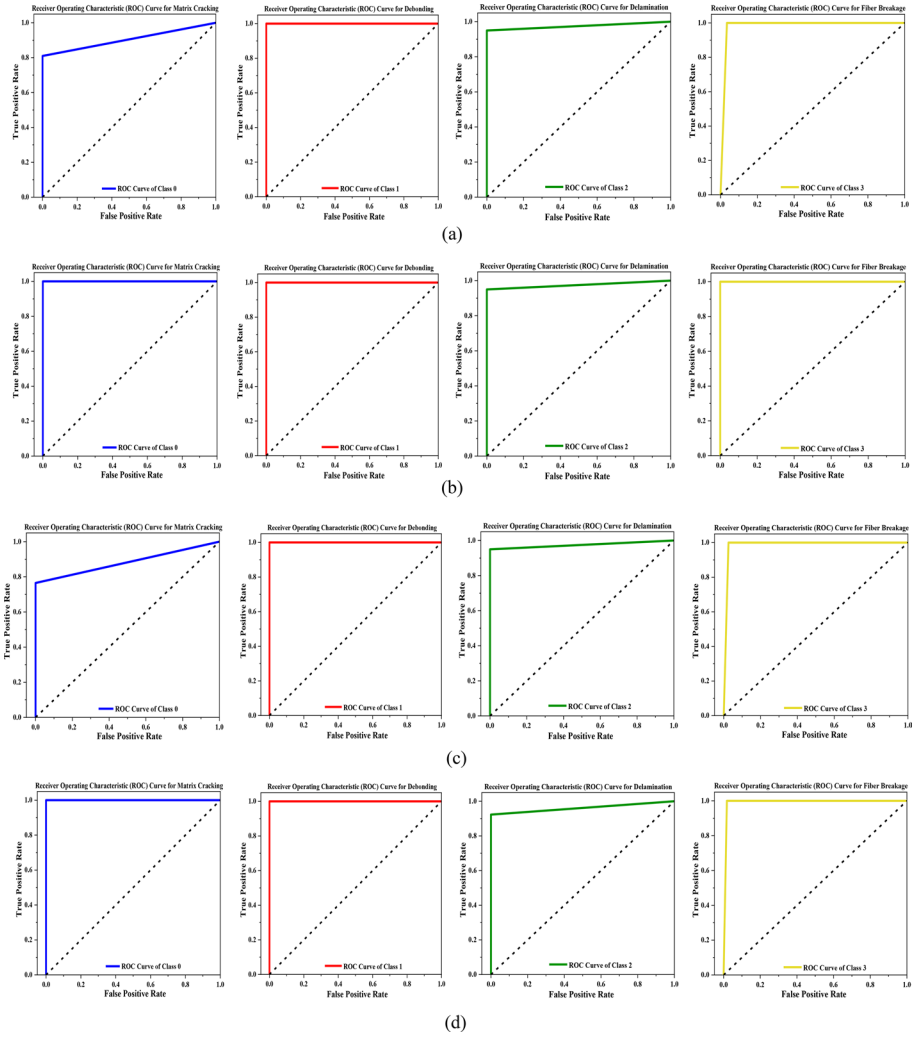

Fig. 8 The Receiver Operating Characteristic curve for each failure mechanism (Blue (Matrix Cracking), Red (Debonding), Green (Delamination), and Yellow(Fiber Breakge)): **a** ANN, **b** Random Forest, **c** SVM, and **d** Naive Bayes

superior performance. Conversely, both the ANN and SVM models exhibited a cumulative count of five within the sub-diagonals of the Confusion Matrix, aligning with the number of disparities observed between the real and predicted graphs. This discrepancy serves to emphasize the relatively weaker performance of ANN and SVM models in comparison to the Random Forest and Naive Bayes models.

The extracted results in the study provided a set of useful information about the performance of each algorithm and the computation time consumption outlined as follows: The detailed analysis of different observed failure mechanisms revealed that four different failure mechanisms occurred during the tests. This information was later utilized for the classification purposes of the failure mechanisms using the hierarchical clustering algorithm as a hyperparameter to determine the failure type. However, as the results revealed

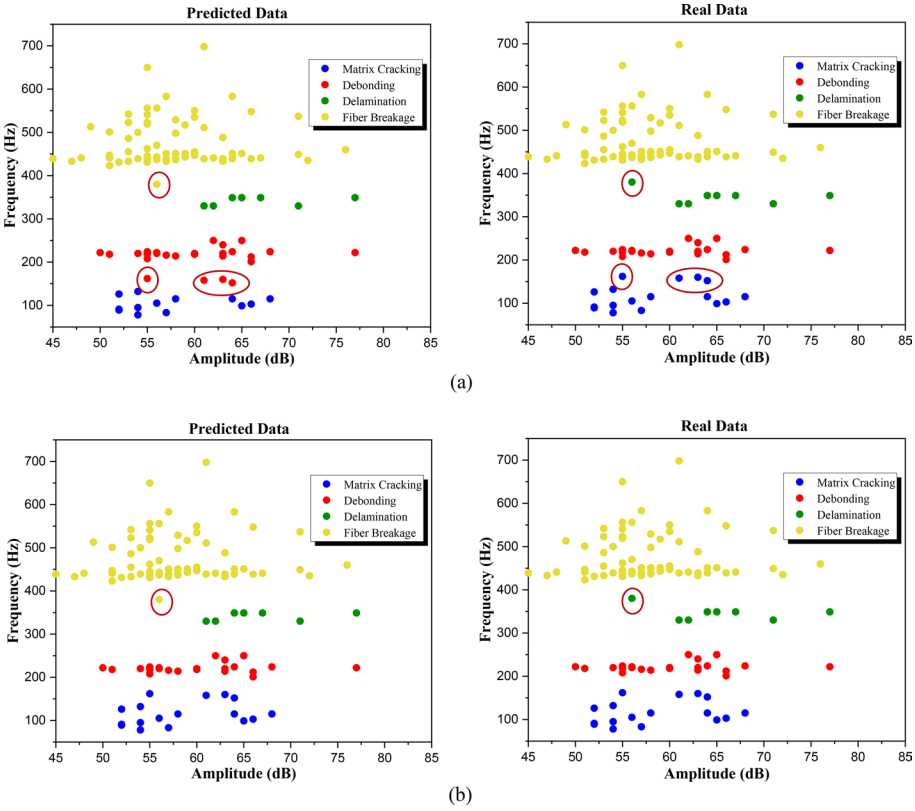

Fig. 9 Comparison between the actual class distribution of the test dataset and the predicted class distribution extracted by the trained: **a** ANN, **b** Random Forest, **c** SVM, and **d** Naive Bayes

the algorithm was unable to classify the data correctly and put them in correct clusters as it separated the data into only three classes. This issue mainly stemmed from the fact that the input features of the collected data in the upper regions of the both input features were close to each other and therefore the algorithm could not separate them from each other. More specifically, the hierarchical algorithm assumed the two failure mechanisms as one entity since the input features were close to each other. Contrary to hierarchical clustering algorithm, Genetic K-means was able to correctly classify the data based on the given input features into four clusters mapping each input feature correctly to the corresponding cluster representing a certain failure mechanism. It was obvious that the Genetic K-means outperformed the hierarchical clustering method in terms of accuracy and performance. Furthermore, despite the previous algorithm, no hyperparameter was provided to the Genetic K-means for the clustering purposes and the algorithm itself was able to figure out the correct number of clusters. This is mainly because of the metaheuristic algorithms within the Genetic K-means and the embedded cost function that helps the algorithm classify all the data correctly in true clusters. Similar to Genetic K-means, ANN was also able to classify the dataset correctly and put them in correct orders with higher train and test accuracy rates. However, despite Genetic K-means the data needed to be labeled for the training purposes of the ANN Algorithm due to its supervised learning behavior. Whereas, in Genetic

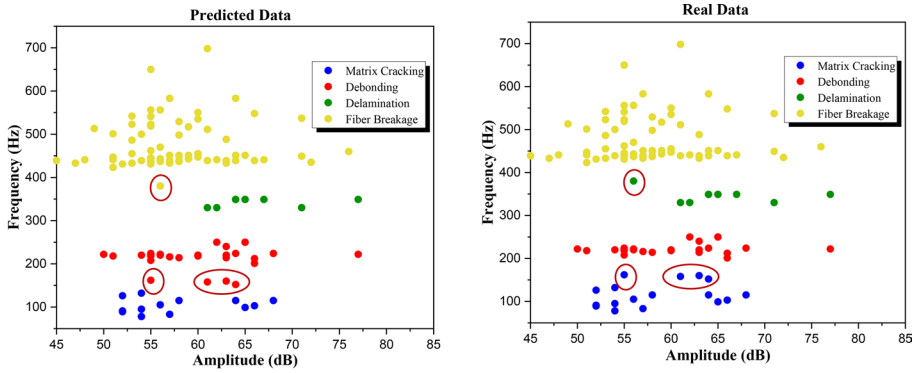

Fig. 9 (continued)

K-means the raw data did not need to be labeled due to the unsupervised behavior of the algorithm and the algorithm could determine the number of clusters by itself through iterative algorithm execution. Nevertheless, the iterative execution of Genetic K-means through all the possible increases the computation time of the algorithm. The same issue persists in ANN as well. More specifically, if the neural network architecture is more complicated or the data at hand is bigger the computation time of the neural network performance will increase to considerable extents lowering the computation time, memory consumption, and performance efficiency yet the performance accuracy will be higher and more accurate. The mentioned computation time and memory consumption issues stated in the previous methods do not have huge effects on the hierarchical clustering method making it more suitable for utilizations yet in the event of a complicated data the algorithm does not guarantee to perform properly in contrast to the other algorithms. Table 7. recapitulates all the algorithms and makes a fair comparison among them.

From the comparison of supervised and unsupervised graphs obtained from both methods with the experimental results of previous research [17], it can be concluded that supervised clusters are generally precise in discovering common failures in composites, but they cannot effectively discover uncharted failures (When data from different failure mechanisms are too close to each other, they do not correctly detect adjacent or near failure boundaries). One of the issues with the supervised approach is that in its retrospective mode, scientists

Table 7 Comparison between different classification algorithms used in this study

	Hierarchical Clustering	Genetic K-means Clustering	Artificial Neural Network
Learning Type	Unsupervised Learning	Unsupervised Learning	Supervised Learning
Hyperparameter tuning for clustering / classification	Required	Not Required	Required
Performance Accuracy	Low	High	High
Computation Time	Low	High	High
Memory allocation	Low	High	High

mostly have to define and clarify experiments related to previous events [39]. That is the reason why their results cannot be simply generalized to the real-time or upcoming state, particularly when failure modes are changing drastically. On the other hand, unsupervised clusters are generally less precise than supervised ones, since their learning procedure does not depend on labeled train information. After all, the precision of unsupervised clusters does not suffer significant demotion in case of unfamiliar failure mechanisms. Also, presumptions required for the supervised method can only be justifiable and lead to decision-making effectiveness for cases where a fair and unprejudiced definition of success can be formulated as an objective function. In contrast, the results demonstrated using an unsupervised method leads to a more reasonable balance of effectiveness and efficiency when the formulation of a fair and unprejudiced definition of success is not possible.

7 Conclusions

In this study, the impact characteristics and damage mechanisms of composite tubes under axial compressive load were assessed using AE monitoring and machine learning methods. The ANN model was compared with Random Forest, SVM, and Naive Bayes models. Matrix cracking, delamination, debonding, and fiber breakage were induced by the bending of the layers. As the failure mode was altered, an increase in fibers/matrix separation and fiber breakage was observed, while a decrease in matrix cracking was noted.

The hierarchical classification method categorized signals into three frequency ranges: 68–200 kHz, 210–350 kHz, and 380 kHz < f, with corresponding dB ranges of 46–81 dB, 50–93 dB, and 45–85 dB. The K-means genetic method clustered the progressive failure mode frequency range into four groups: 68–166 kHz, 173–269 kHz, 310–386 kHz, and frequencies greater than 404 kHz. The K-means genetic method distinguished fibers/matrix separation (81–50 dB) from interlaminar separation (61–93 dB) failure modes more accurately than the hierarchical method.

The ANN model, using amplitudes and frequencies as input features, exhibited higher accuracy in classifying data, with each class representing a specific failure mechanism. The Random Forest model consistently outperformed the ANN and SVM models, demonstrating superior predictive accuracy across multiple evaluation metrics. It achieved higher true positive rates and lower false positive rates compared to the other models. The predicted class distribution analysis further substantiated the superiority of the Random Forest model, closely aligning with the actual class distribution. In conclusion, our comprehensive

evaluation highlighted the Random Forest model's superior performance in terms of predictive accuracy and classification using ACC, MCC and F1-Score metrics. These findings contribute to the understanding of model selection and performance assessment in machine learning, providing valuable insights for future research and practical applications.

The quantitative assessment of each failure mechanism can enhance the failure efficiency of composite structures by controlling the proportion of damage mechanisms. Future work will focus on optimizing algorithms for failure detection in different composites and shapes, enabling robust failure detection using machine learning techniques, even without explicit information about failures in the training data.

Author Contributions All authors have made significant contributions to the research presented in this manuscript. They have reviewed and approved the contents of the manuscript and have agreed to adhere to ethical standards.

Funding This research was not supported by any specific grants from public, commercial, or not-for-profit funding agencies.

Data Availability Statements The authors can confirm that all data generated or analyzed during this study are included in the article and/or its supplementary information files.

Declarations

Ethical Approval This manuscript is an original work and has not been previously submitted, either partially or in full, for publication elsewhere. Furthermore, it has not been simultaneously submitted to multiple publications for consideration.

Conflict of Interest The authors declared that they have no conflicts of interest in this work.

References

1. Thirumavalavan, K., Sarukasan, D.: Experimental investigation on multi-layered filament wound basalt/E-glass hybrid fiber composite tubes. Mater. Res. Express. **9**(4), (2022)
2. Bani Mohammad Ali, A., Alimirzaei, S., Ahmadi Najafabadi, M.: Evaluation of damage of filament wound composite tubes under lateral loading by acoustic emission method and finite element simulation. Modares. Mech. Eng. **22**(11), 647–655 (2022)
3. Mohamad, F., Hossein, H., Farzad, P., Ahmadi Najaf Abadi, M.: Composite materials damage characterization under quasi-static 3-point bending test using fuzzy C-means clustering. Appl. Mech. Mater. Trans. Tech. Publ. 1221–1228 (2012)
4. Ameur, M.B., El Mahi, A., Rebiere, J.-L., Gimenez, I., Beyaoui, M., Abdennadher, M., Haddar, M.: Investigation and identification of damage mechanisms of unidirectional carbon/flax hybrid composites using acoustic emission. Eng. Fract. Mech. **216**, 106511 (2019)
5. Beheshtizadeh, N., Mostafapour, A., Davoodi, S.: Three point bending test of glass/epoxy composite health monitoring by acoustic emission. Alex. Eng. J. **58**(2), 567–578 (2019)
6. Jung, K.-C., Chang, S.-H.: Advanced deep learning model-based impact characterization method for composite laminates. Compos. Sci. Technol. **207**, 108713 (2021)
7. Azizian, M., Almeida, J.H.S., Jr.: Stochastic, probabilistic and reliability analyses of internally-pressurised filament wound composite tubes using artificial neural network metamodels. Mater. Today Commun. **31**, 103627 (2022)
8. Šofer, M., Cienciala, J., Fusek, M., Pavlíček, P., Moravec, R.: Damage analysis of composite CFRP tubes using acoustic emission monitoring and pattern recognition approach. Materials **14**(4), 786 (2021)
9. Park, D., Jung, J., Gu, G.X., Ryu, S.: A Generalizable and Interpretable Deep Learning Model to Improve the Prediction Accuracy of Strain Fields in Grid Composites. Mater. Des. 111192 (2022)

10. Cui, R., Azuara, G., Lanza di Scalea, F., Barrera, E.: Damage imaging in skin-stringer composite aircraft panel by ultrasonic-guided waves using deep learning with convolutional neural network. Struct. Health Monit. **21**(3), 1123–1138 (2022)
11. Kinga, D., Baadam, J.: A method for stochastic optimization, vol. 5, p. 6. International conference on learning representations (ICLR) (2015)
12. Seventekidis, P., Giagopoulos, D.: A combined finite element and hierarchical Deep learning approach for structural health monitoring: Test on a pin-joint composite truss structure. Mech. Syst. Signal Process. **157**, 107735 (2021)
13. Lyu, J., Akhavan, J., Manoochehri, S.: Image-based dataset of artifact surfaces fabricated by additive manufacturing with applications in machine learning. Data Brief **41**, 107852 (2022)
14. Lyu, J., Akhavan Taheri Boroujeni, J., Manoochehri, S.: In-situ laser-based process monitoring and in-plane surface anomaly identification for additive manufacturing using point cloud and machine learning, International Design Engineering Technical Conferences and Computers and Information in Engineering Conference. Ame. Soc. Mech. Eng. V002T02A030 (2021)
15. Azimirad, V., Sotubadi, S.V., Nasirlou, A.: Vision-based Learning: a novel machine learning method based on convolutional neural networks and spiking neural networks, 2021 9th RSI International Conference on Robotics and Mechatronics (ICRoM). IEEE. 192–197 (2021)
16. Zhao, Y., Noori, M., Altabey, W.A., Ghiasi, R., Wu, Z.: Deep learning-based damage, load and support identification for a composite pipeline by extracting modal macro strains from dynamic excitations. Appl. Sci. **8**(12), 2564 (2018)
17. Alimirzaei, S., Najafabadi, M.A., Nikbakht, A., Pahlavan, L.: Damage mechanism characterization of $\pm 35°$ and $\pm 55°$ FW composite tubes using acoustic emission method. 10567895221095603 (2022)
18. Alimirzaei, S., Ahmadi Najafabadi, M., Nikbakht, A., Pahlavan, L.: Investigation of energy absorption capacity of 3D filament wound composite tubes: experimental evaluation, numerical simulation, and acoustic emission monitoring. Mech. Adv. Mater. Struct. 1–16 (2023)
19. Saeedifar, M., Zarouchas, D.: Damage characterization of laminated composites using acoustic emission: A review. Compos. B Eng. **195**, 108039 (2020)
20. Yousefi, J., Najfabadi, M.A., Toudeshky, H.H., Akhlaghi, M.: Damage evaluation of laminated composite material using a new acoustic emission Lamb-based and finite element techniques. Appl. Compos. Mater. **25**, 1021–1040 (2018)
21. Fotouhi, M., Suwarta, P., Jalalvand, M., Czel, G., Wisnom, M.R.: Detection of fibre fracture and ply fragmentation in thin-ply UD carbon/glass hybrid laminates using acoustic emission. Compos. A Appl. Sci. Manuf. **86**, 66–76 (2016)
22. Kumar, C.S., Arumugam, V., Sajith, S., Dhakal, H.N., John, R.: Acoustic emission characterisation of failure modes in hemp/epoxy and glass/epoxy composite laminates. J. Nondestr. Eval. **34**, 1–11 (2015)
23. Woo, S.-C., Kim, T.-W.: High-strain-rate impact in Kevlar-woven composites and fracture analysis using acoustic emission. Compos. B Eng. **60**, 125–136 (2014)
24. Nimdum, P., Renard, J.: Use of acoustic emission to discriminate damage modes in carbon fibre reinforced epoxy laminate during tensile and buckling loading, ECCM 15–15th European Conference on Composite Mater. 8 (2012)
25. Ni, Q.-Q., Iwamoto, M.: Wavelet transform of acoustic emission signals in failure of model composites. Eng. Fract. Mech. **69**(6), 717–728 (2002)
26. Saeedifar, M., Najafabadi, M.A., Zarouchas, D., Toudeshky, H.H., Jalalvand, M.: Clustering of interlaminar and intralaminar damages in laminated composites under indentation loading using Acoustic Emission. Compos. B Eng. **144**, 206–219 (2018)
27. Gutkin, R., Green, C., Vangrattanachai, S., Pinho, S., Robinson, P., Curtis, P.: On acoustic emission for failure investigation in CFRP: Pattern recognition and peak frequency analyses. Mech. Syst. Signal Process. **25**(4), 1393–1407 (2011)
28. Chou, H.-Y., Mouritz, A., Bannister, M., Bunsell, A.R.: Acoustic emission analysis of composite pressure vessels under constant and cyclic pressure. Compos. A Appl. Sci. Manuf. **70**, 111–120 (2015)
29. De Groot, P.J., Wijnen, P.A., Janssen, R.B.: Real-time frequency determination of acoustic emission for different fracture mechanisms in carbon/epoxy composites. Compos. Sci. Technol. **55**(4), 405–412 (1995)
30. Liu, P., Chu, J., Liu, Y., Zheng, J.: A study on the failure mechanisms of carbon fiber/epoxy composite laminates using acoustic emission. Mater. Des. **37**, 228–235 (2012)
31. Ceysson, O., Salvia, M., Vincent, L.: Damage mechanisms characterization of carbon fiber/epoxy composite laminates by both electrical resistance measurements and acoustic emission analysis. Scripta. Materialia. **34**(8), (1996)
32. Bourchak, M., Farrow, I., Bond, I., Rowland, C., Menan, F.: Acoustic emission energy as a fatigue damage parameter for CFRP composites. Int. J. Fatigue **29**(3), 457–470 (2007)

33. Morissette, L., Chartier, S.: The k-means clustering technique: General considerations and implementation in Mathematica. Tutorials in Quantitative Methods for Psychology **9**(1), 15–24 (2013)
34. Hartigan, J.A., Wong, M.A.: Algorithm AS 136: A k-means clustering algorithm J. R. Stat. Soc. Ser. C Appl. Stat. **28**(1), 100–108 (1979)
35. Murtagh, F.: A survey of recent advances in hierarchical clustering algorithms. Comput. J. **26**(4), 354–359 (1983)
36. Alimirzaei, S., Najafabadi, M.A., Ali, A.B.M.: Investigation of Failure Mechanism of the Composite Tubes Made by Filament Winding Process by Acoustic Emission Method. Amirkabir J. Mech. Eng. **54**(6), 1357–1372 (2022)
37. Boominathan, R., Arumugam, V., Santulli, C., Sidharth, A.A.P., Sankar, R.A., Sridhar, B.: Acoustic emission characterization of the temperature effect on falling weight impact damage in carbon/epoxy laminates. Compos. B Eng. **56**, 591–598 (2014)
38. Mohammadi, M., Saidi, A.R., Jomehzadeh, E.: A novel analytical approach for the buckling analysis of moderately thick functionally graded rectangular plates with two simply-supported opposite edges. Proc. Inst. Mech. Eng. C J. Mech. Eng. Sci. **224**(9), 1831–1841 (2010)
39. Lee, K., Booth, D., Alam, P.: A comparison of supervised and unsupervised neural networks in predicting bankruptcy of Korean firms. Expert Syst. Appl. **29**(1), 1–16 (2005)